Microbunched Electron Cooling for High-Energy Hadron Beams

D. Ratner*

SLAC, Menlo Park, California 94025, USA

(Received 11 April 2013; published 20 August 2013)

Electron and stochastic cooling are proven methods for cooling low-energy hadron beams, but at present there is no way of cooling hadrons as they near the TeV scale. In the 1980s, Derbenev suggested that electron instabilities, such as free-electron lasers, could create collective space charge fields strong enough to correct the hadron energies. This Letter presents a variation on Derbenev's electron cooling scheme using the microbunching instability as the amplifier. The large bandwidth of the instability allows for faster cooling of high-density beams. A simple analytical model illustrates the cooling mechanism, and simulations show cooling rates for realistic parameters of the Large Hadron Collider.

DOI: 10.1103/PhysRevLett.111.084802 PACS numbers: 29.27.−a, 41.60.Cr, 41.75.Ak, 41.75.Ht

The ability to cool high-energy hadron beams would benefit both future collider projects, where luminosity is in part determined by energy spread (see, e.g., Ref. [1]), as well as hadron-based plasma accelerators [2]. Unfortunately, traditional particle cooling methods are not effective for hadron beams in the TeV energy range. Though synchrotron radiation quickly cools electrons, even at 7 TeV the protons at the Large Hadron Collider (LHC) have negligible radiative cooling. Electron cooling, which has successfully cooled hadron beams below 10 GeV, is ineffective at the TeV scale [3,4]. An alternative approach is stochastic cooling, in which an rf pickup measures particle properties and a subsequent kicker stage adjusts the particles towards the beam's mean value [5]. However, the limited rf bandwidth cannot accommodate the high-density bunched beams used at either the LHC or the Relativistic Heavy Ion Collider (see, e.g., Ref. [6]). (Optical stochastic cooling has been proposed to adapt stochastic cooling to bunched beams; the optical wavelengths support higher bandwidths in both the pickup and kicker stages, allowing faster cooling of high density beams [7]). More than two decades ago, Derbenev merged ideas from classic stochastic and electron cooling, proposing the coherent electron cooling (CeC) scheme in which an electron beam serves as both the pickup and kicker (see, e.g., Refs. [8,9]). To increase the CeC cooling rate, a free-electron laser (FEL) can amplify the electron signal between the pickup and kicker [10,11]. The FEL creates a periodic density modulation of the electrons, and the resulting Coulomb fields adjust the hadron energies inside the kicker. Studies of CeC for cooling both the Relativistic Heavy Ion Collider and the LHC are under way (see, e.g., Ref. [12]).

CeC benefits from the large bandwidth of an ultraviolet FEL but produces a series of periodic density spikes of which only one contributes to cooling; ideally, the amplification process would create just the single spike needed to cool each hadron. In this Letter, we propose an alternative hadron cooling scheme using the microbunching instability (MBI) from longitudinal space charge as an amplifier. In longitudinal space charge-driven MBI, space charge from an initial density modulation causes an energy modulation, which a dispersive region then converts back into an amplified density modulation (see, e.g., Refs. [13,14]). Though primarily studied as a detrimental instability, MBI can also be used to intentionally amplify an initial modulation [15,16]. In this cooling scheme, a hadron's Coulomb field produces the initial electron energy modulation. A dispersive region then converts the energy modulation from each hadron into a single density spike and, as in CeC, each density spike adjusts the energy of its corresponding hadron in a kicker. (We note that a dispersive section was first introduced by Litvinenko to accelerate the plasma oscillation in CeC prior to the amplification stage [10]. Here we use the dispersion as the amplifier itself). Microbunched electron cooling (henceforth, MBEC) offers two benefits. First, the instability creates only a single density spike for each hadron, maximizing the bandwidth of the amplifier. The large amplifier bandwidth is crucial for cooling high-density bunched beams, such as those at the LHC. Second, the scheme is relatively simple, consisting only of drift and dispersive regions.

Figure 1 provides a schematic of a one-dimensional MBEC model. In the first section, the Coulomb field of a hadron (e.g., an ion) modulates the electron energies. Electrons and ions take separate paths in the second section, where dispersion converts the electron energy modulation into a density spike at the ion's former location. In the third section, the ions return to the electron beam. An ion with lower-than-average energy falls behind the spike it created, and the collective electron field provides an energy boost; conversely, an ion with above-average energy slips ahead of its spike, and the collective electron field pulls the ion backwards. The net effect is to push all ions towards the average energy, i.e., cooling. In practice, the process must be repeated many times as the hadron beam circulates in a storage ring. This Letter focuses on longitudinal cooling, but as described in Ref. [11], it is

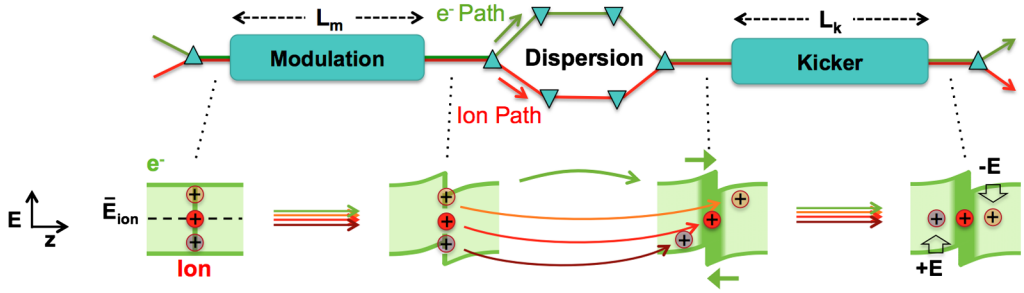

FIG. 1 (color online). Schematic of the cooling mechanism. In the first stage, an ion modulates the energy of the local electrons. In the dispersive region, ions and electrons move longitudinally due to energy differences, creating an electron density spike at the overlap. In the kicker stage, an ion with nominal energy $E = \bar{E}_{\rm ion}$ (red, middle) returns to the center of the spike and does not change energy. A low energy ion with $E < \bar{E}_{\rm ion}$ (purple, lower) falls behind its original position, and receives a positive energy kick from the electron spike. A high energy ion with $E > \bar{E}_{\rm ion}$ (orange, upper) slips ahead of its electron spike and receives a negative energy kick. The result is that all ions are pushed towards the average ion energy.

straightforward to extend cooling to the transverse dimensions as well.

To describe MBEC analytically, we start by considering the effect on the electron beam from an ion of charge q. We assume ion and electron beams each have an average relativistic Lorentz factor $\gamma \gg 1$ corresponding to an average electron energy $\bar{E}_e = \gamma m_e c^2$ and average ion energy $\bar{E}_{\rm ion} = \gamma m_I c^2$. We consider an electron that starts with longitudinal position z and relative energy $p \equiv (E - \bar{E}_e)/\bar{E}_e$. We consider two possible cases. First, we assume that the electron's energy modulation due to the ion occurs over a length, L_m, that is long compared to the β function. In this case, the electron moves transversely during the interaction, washing out transverse structure, so we can treat each electron as a circular disc of charge e and radius a [17]. For simplicity, we assume the ion sits at the center of the bunch ($r = 0$, $z = 0$). An electron at position z then experiences a relative energy shift due to the ion's Coulomb field of [10]

$$M(z) = \frac{-2cqL_m}{\gamma a^2 I_A}\left[\frac{z}{|z|} - \frac{\gamma z}{\sqrt{a^2 + \gamma^2 z^2}}\right], \tag{1}$$

with Alfven current $I_A \equiv 4\pi\epsilon_0 m_e c^3/e$. An electron with initial position z then has a final longitudinal coordinate in the kicker (following both the modulation and dispersive regions) of

$$\tilde{z} = z + R_{56}[M(z) + p]. \tag{2}$$

In the same way that the ion changes the electron energies in the modulator [Eq. (1)], the total Coulomb field of the final electron distribution corrects the ion energy in the kicker. Summing the kicks from each of the N electrons in the bunch, an ion at longitudinal position z_I experiences a total energy shift

$$W(z_I) = \sum_j^N \frac{-qeL_k}{2\epsilon_0 \pi a^2}\left[\frac{z_I - \tilde{z}_j}{|z_I - \tilde{z}_j|} - \frac{\gamma(z_I - \tilde{z}_j)}{\sqrt{a^2 + \gamma^2(z_I - \tilde{z}_j)^2}}\right], \tag{3}$$

with kicker length L_k and final position of the jth electron $\tilde{z}_j$. To find the expectation value $\langle W(z_I)\rangle$, we assume a uniform and uncorrelated initial electron distribution. For a cylindrical beam with current I, radius a, and rms energy spread σ_p, we replace the sum in Eq. (3) with an integral over $\Psi(z, p) = (I/ec\sqrt{2\pi}\sigma_p)\exp[-p^2/2\sigma_p^2]$. Defining the modulation strength factor $A_1 \equiv -2cqL_m/a^2 I_A$ and kicker strength factor $A_2 \equiv -qIL_k/2\epsilon_0 c\pi a^2$, it is convenient to work in dimensionless variables $\zeta \equiv \gamma z/|R_{56}A_1|$, $\alpha \equiv a/|R_{56}A_1|$, $\xi \equiv \gamma p/|A_1|$, and $\sigma_\xi \equiv \gamma\sigma_p/|A_1|$ to find the final electron position

$$\tilde{\zeta}(\zeta, \xi) \equiv \zeta\left[1 - \frac{s}{|\zeta|} + \frac{s}{\sqrt{\alpha^2 + \zeta^2}}\right] + s\xi, \tag{4}$$

and corresponding energy shift

$$\langle W_I(z_I)\rangle = \frac{|R_{56}A_1|A_2}{\gamma}\int_{-\infty}^{\infty} d\xi \frac{e^{-\xi^2/2\sigma_\xi^2}}{\sqrt{2\pi}\sigma_\xi}\int_{-\infty}^{\infty} d\zeta \times\left(t(\zeta, \xi) - \frac{[\zeta_I - \tilde{\zeta}(\zeta, \xi)]}{\sqrt{\alpha^2 + [\zeta_I - \tilde{\zeta}(\zeta, \xi)]^2}}\right), \tag{5}$$

where we have used shorthands $s \equiv \mathrm{sgn}(R_{56})$ and $t(\zeta, \xi) \equiv \mathrm{sgn}[\zeta_I - \tilde{\zeta}(\zeta, \xi)]$. The optimal R_{56} is determined by balancing the desired gain against the damping that results from slice energy spread, as well as practical experimental limits. It is interesting to note that cooling is possible with either positive or negative R_{56}, though the sign of the gain and the ion's dispersion also switch.

In the previous analysis, we assumed that the modulation length was long compared to the electron β function, $L_m \gg \beta$, so we treated each electron as a circular disc of radius a. If we take the opposite limit, $L_m \ll \beta$, then we treat each electron as a point charge at position r, z. (To simplify, we again assume the ion is at $r = 0$, $z = 0$). In the point-charge limit, an electron's relative energy shift due to the ion is

$$M(r,z) = \frac{-cqL_m}{\gamma I_A}\frac{\gamma z}{[r^2+\gamma^2 z^2]^{3/2}}. \quad (6)$$

We can notice that for electrons in the region $|\gamma z| \ll r$, the energy shift is linear in the initial longitudinal position so that $\tilde{z} \approx z(1 + B_1 R_{56}/r^3)$ with modulation strength factor now defined as $B_1 \equiv -cqL_m/I_A$. The result is that electrons at a radius $r_{\text{spike}} \equiv |B_1 R_{56}|^{1/3}$ move to $\tilde{z} = 0$, creating a ring of high density. Redefining the kicker strength parameter $B_2 \equiv -qIL_k/2\epsilon_0 c(\pi a^2)^2$ and dimensionless coordinates, $\rho = r/r_{\text{spike}}$, $\zeta \equiv \gamma z/r_{\text{spike}}$, $\zeta_I \equiv \gamma z_I/r_{\text{spike}}$, $\tilde{\zeta} \equiv \gamma\tilde{z}/r_{\text{spike}}$, $\alpha \equiv a/r_{\text{spike}}$, $\xi \equiv \gamma|R_{56}|p/r_{\text{spike}}$, and $\sigma_\xi \equiv \gamma|R_{56}|\sigma_p/r_{\text{spike}}$ gives the final longitudinal positions

$$\tilde{\zeta}(\zeta,\rho,\xi) = \zeta[1 - s(\rho^2+\zeta^2)^{-3/2}] + s\xi. \quad (7)$$

The corresponding ion energy shift in the point-charge limit is again given by Eq. (5) but with an additional integral over the transverse coordinates. The need to keep $L_m \ll \beta$ may make the disc limit more practical, and for simplicity, we will consider only the disc limit for the rest of this Letter.

In stochastic cooling, the pickup samples all particles in the beam; in MBEC, the Coulomb fields of all electrons and ions contribute equally to the energy modulation, which can both heat the electron beam (see, e.g., Ref. [18]) and create random density spikes that heat the ions in the kicker. For example, assuming the particles are initially uncorrelated, shot noise from the modulator produces additional electron energy spread at $z = 0$ of

$$\sigma_{p\text{SN}}^2 = \left\langle\left[\sum_j^N M(z_j)\right]^2\right\rangle = \frac{I_T}{ec}\int_{-\infty}^{\infty} dz[M(z)]^2$$
$$\Rightarrow \sigma_{p\text{SN}} \approx 0.93\frac{A_1}{\gamma}\sqrt{\frac{I_T}{ec}\frac{a}{\gamma}}, \quad (8)$$

with $I_T \equiv I_e + I_I$ the total current of both ions and electrons. More critically, the shot noise energy modulation is amplified by the MBEC process, resulting in random spikes that heat the ion in the kicker. If the amplifier does not saturate, each particle contributes a kick to the ion of $W_e(z)$ or $W_I(z)$ and the ion experiences a random kick of amplitude

$$\Delta E_{\text{SN}} = \sqrt{\frac{1}{ec}\int_{-\infty}^{\infty} dz[I_e\langle W_e(z)\rangle^2 + I_I\langle W_I(z)\rangle^2]}. \quad (9)$$

The electron kick $W_e(z)$ can be found from the MBI gain [18]. The shot noise spikes should not be allowed to saturate, which sets a limit on the total amplification factor.

So far we have only considered a single modulation-dispersive region (Fig. 1). Figure 2 shows a variation with additional modulation-dispersive stages that both increase the cooling rate and improve tolerances. In the subsequent amplification stages, the ion and electron beams do not interact; the electron density modulation of the first stage drives the gain as in a longitudinal space charge amplifier [15,16]. Each dispersive region can be either positive or negative, but in practice, setting the total dispersion $R_{56}^{(T)} \sim 0$ minimizes timing errors from electron beam energy jitter.

To fully incorporate shot noise into MBEC, we implement a custom particle-tracking simulation. The simulation places a single ion at the center of a cylindrical electron beam with Gaussian energy spread and the real number of particles. In the modulation stage, the electrons change energy according to the collective Coulomb field of both the ion and the electrons [Eq. (1)]. Because of the large γ, we neglect longitudinal motion during the modulation. Periodic boundary conditions allow simulation of a short bunch. In the dispersive region, R_{56} moves electrons longitudinally. Additional amplification stages repeat this process but without the ion field and with opposite sign R_{56}. The electron-electron interaction is more precisely calculated as the field between two discs, but in practice the simpler expression in Eq. (1) gives a nearly identical result and is computationally less expensive. Finally, we calculate the collective Coulomb field along the bunch axis ($r = 0$) to determine the energy shift experienced by the ion.

For large high-current beams, the simulation becomes prohibitively computationally expensive. However, if ΔE_{SN} does not saturate (so the amplification is linear), then we can treat the electron beam as a uniform fluid

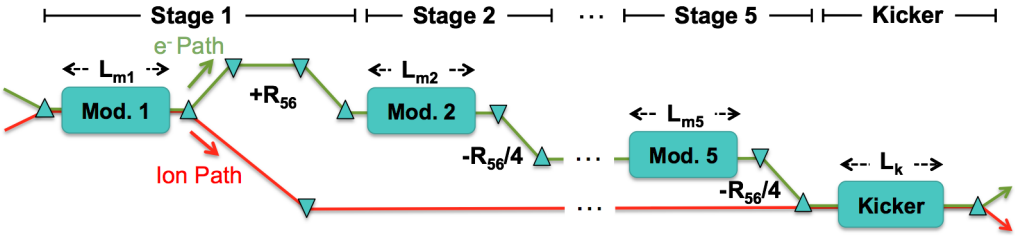

FIG. 2 (color online). Schematic of a five-stage MBEC. After the ion-electron interaction, four identical electron-only stages amplify the initial density modulation. The additional stages both increase the cooling rate and force $R_{56}^{(T)} = 0$, reducing the relative timing jitter of the electron and ion beams.

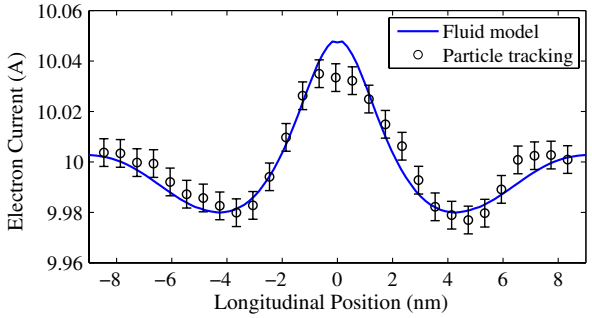

FIG. 3 (color online). Comparison between the full particle-tracking simulation and the fluid model without shot noise shows convergence after 500 000 passes. Parameters are taken from Table I but with $a = 25, 9$ μm, $I = 10$ A, and $\sigma_p = 2.5 \times 10^{-5}$ due to computational constraints. The smaller beam size and energy spread of this toy case make simulation easier but increase the gain, leading to shot noise saturation and a slight discrepancy at the peak.

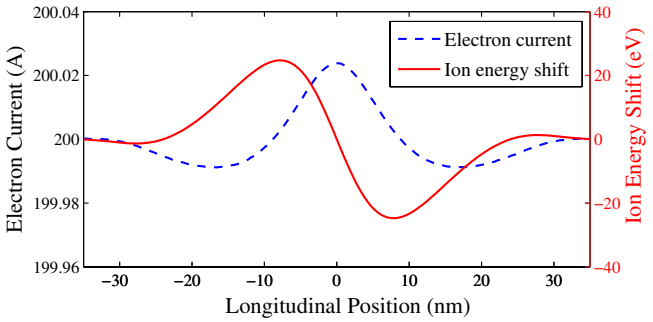

FIG. 4 (color online). Blue dashed line shows the final electron current from a fluid model without shot noise for LHC-like parameters of Table I. The corresponding ion energy shift (solid red line) has a maximum change of 25 eV per pass.

and ignore shot noise when calculating the average density. Figure 3 shows a comparison between a simulation including shot noise and the fluid model. To facilitate the shot noise simulation, we use only the central portion of the beam (1/4 by radius) and also reduce the energy spread by a factor of 4. Otherwise, the parameters are the same as in Table I.

To estimate the cooling rate of an LHC-like machine, we use the fluid model to simulate the parameters of Table I. The maximum energy shift per turn is given by the peak amplitude of the solid curve in Fig. 4. With a rms energy spread of 800 MeV, cooling the LHC beam requires around 3×10^7 passes or a little less than one hour. Table I is not an optimized parameter set, and faster cooling rates may be possible. Ideally, the electron beam covers the entire ion beam on every turn, requiring a 50 nC, 250 ps electron bunch for the case of Table I. Cooling will be slower if it is necessary to ''paint'' the electron beam across a larger ion beam [11].

Both electrons and ions randomize each revolution around the ring, so the cooling effect of the ion's self-generated kick W_{I} dominates after many turns despite having $W_{\mathrm{I}} \ll \Delta E_{\mathrm{SN}}$. With an adjustable ion dispersion [19,20], the fundamental limit on the equilibrium energy spread is $\sigma_{p0} \approx \Delta E_{\mathrm{SN}}^2 / 2 W_{\mathrm{I}} \sim 10$ MeV for the example of Fig. 4. Turning down the longitudinal space charge amplifier gain during cooling can produce even smaller σ_{p0}. In principle, it should be possible to mitigate electron shot noise effects (and thus heating) with dispersive noise suppression in the first modulation region [21,22]. (Noise suppression can improve CeC as well [23]). In practice, the minimum energy spread at the LHC is limited by other effects (see, e.g., Ref. [24]). However, even a moderate degree of cooling in either the longitudinal or transverse planes could improve the LHC's performance.

MBEC will face a number of technological challenges. Conventional linacs can satisfy the parameters in Table I (see, e.g., Ref. [25]), but an energy recovery linac may be necessary to match the LHC's MHz bunch rate [26,27]. Electron storage rings are naturally suited for high repetition rates but typically have larger slice energy spread and emittance. To create a smaller effective slice energy spread for a storage ring, it may be possible to either stretch the beam longitudinally or place the entire MBEC process inside a dispersive region [28,29]. The ion and electron energy difference, $\Delta\gamma \equiv \gamma_e - \gamma_I$, must be small to limit the relative slippage of $\Delta z \approx L_m \Delta\gamma / \gamma^3$. The ion energy shift in Fig. 4 has a FWHM length of 30 nm, so timing and stability of the ion delay could be challenging. Emittance effects will tend to wash out cooling, but should be manageable; for example, assuming 2 μm emittance and

TABLE I. LHC-like parameters for the case of Fig. 4. Note that these parameters are only an example; except for γ (which is determined by the ion energy), trade-offs between parameters are possible while maintaining the same gain.

Example parameters	Stage 1	Stages 2–5	Kicker
Relativistic factor (γ)		7000	
Electron current (I)		200 A	
Electron slice energy spread (σ_p)		1×10^{-4}	
Electron beam radius (a)	100 μm	35 μm	100 μm
Dispersion (R_{56})	100 μm	4×-25 μm	NA
Interaction length (L_m)	25 m	4×25 m	25 m

Table I parameters, β oscillations in each stage will randomize longitudinal particle positions by less than 1 nm. Increased energy spread from synchrotron radiation in the bends should also be considered.

We conclude that MBEC is a potentially feasible scheme for cooling high-energy ion beams. A numerical solution for an LHC-like case shows that cooling is fast compared to the bunch storage time and could lower the energy spread and emittance of collider experiments or improve advanced acceleration techniques. While the electron beam requirements are challenging, the tolerances are similar to those of FEL-based CeC. The next step is to perform detailed massively parallel simulations, including particle motion during the modulation process and to investigate machine tolerances for a practical example.

The author would like to thank N. P. Breznay, A. Chao, V. Litvinenko, A. Marinelli, T. Mastoridis, G. Wang, D. Xiang, and M. Zolotorev for their insightful comments. The author is particularly indebted to G. Stupakov who provided numerous suggestions and discussions throughout the development of the Letter. Research is supported by the U.S. Department of Energy under Contract No. DE-AC02-76SF00515. Simulations completed at the National Energy Research Scientific Computing Center, which is supported by the U.S. Department of Energy Office of Science under Contract No. DE-AC02-05CH11231.

*dratner@slac.stanford.edu

[1] L. Rossi, in *Proceedings of IPAC2011, San Sebastian, Spain, 2011*.
[2] A. Caldwell, K. Lotov, A. Pukhov, and F. Simon, Nat. Phys. **5**, 363 (2009).
[3] G. I. Budker, Sov. At. Energy **22**, 438 (1967).
[4] S. Nagaitsev *et al.*, Phys. Rev. Lett. **96**, 044801 (2006).
[5] S. V. de Meer, Rev. Mod. Phys. **57**, 689 (1985).
[6] F. Caspers and D. Mohl, in *17th International Conference on High Energy Accelerators, Dubna, Russia, 1998*, p. 397.
[7] A. A. Mikhailichenko and M. S. Zolotorev, Phys. Rev. Lett. **71**, 4146 (1993).
[8] Y. S. Derbenev, in *Proceedings of AIP 253* (AIP, College Park, MD, 1992), pp. 103–110.
[9] Y. S. Derbenev, in *Proceedings of COOL, Bad Kreuznach, Germany, 2007*.
[10] V. N. Litvinenko, in *Proceedings of the 2007 FEL Conference, Novosibirsk, Russia, 2007*.
[11] V. N. Litvinenko and Y. S. Derbenev, Phys. Rev. Lett. **102**, 114801 (2009).
[12] I. Pinayev *et al.*, in *Proceedings of IPAC2012, New Orleans, USA, 2012*.
[13] E. L. Saldin, E. A. Schneidmiller, and M. V. Yurkov, Nucl. Instrum. Methods Phys. Res., Sect. A **490**, 1 (2002).
[14] R. Akre *et al.*, Phys. Rev. ST Accel. Beams **11**, 030703 (2008).
[15] E. A. Schneidmiller and M. V. Yurkov, Phys. Rev. ST Accel. Beams **13**, 110701 (2010).
[16] A. Marinelli, E. Hemsing, M. Dunning, D. Xiang, S. Weathersby, F. O'Shea, I. Gadjev, C. Hast, and J. B. Rosenzweig, Phys. Rev. Lett. **110**, 264802 (2013).
[17] A. Marinelli and J. B. Rosenzweig, Phys. Rev. ST Accel. Beams **13**, 110703 (2010).
[18] Z. Huang, J. Wu, and T. Shaftan, http://icfa-usa.jlab.org/archive/newsletter/icfa_bd_nl_38.pdf.
[19] M. S. Zolotorev and A. A. Zholents, Phys. Rev. E **50**, 3087 (1994).
[20] A. Zholents, Phys. Rev. ST Accel. Beams **15**, 032801 (2012).
[21] D. Ratner, Z. Huang, and G. Stupakov, Phys. Rev. ST Accel. Beams **14**, 060710 (2011).
[22] D. Ratner and G. Stupakov, Phys. Rev. Lett. **109**, 034801 (2012).
[23] V. Litvinenko, in *Proceedings of the 2009 FEL Conference, Liverpool, UK, 2009*.
[24] P. Baudrenghien and T. Mastoridis, Nucl. Instrum. Methods Phys. Res., Sect. A **726**, 181 (2013).
[25] P. Emma *et al.*, Nat. Photonics **4**, 641 (2010).
[26] M. Tigner, Nuovo Cimento **37**, 1228 (1965).
[27] G. Neil *et al.*, Phys. Rev. Lett. **84**, 662 (2000).
[28] T. Smith, J. Madey, L. Elias, and D. Deacon, J. Appl. Phys. **50**, 4580 (1979).
[29] Z. Huang, Y. Ding, and C. B. Schroeder, Phys. Rev. Lett. **109**, 204801 (2012).